CHEMISTRY OF MATERIALS

Article

pubs.acs.org/cm

Simultaneous Chemical Modification and Structural Transformation of Stöber Silica Spheres for Integration of Nanocatalysts

Ke Xin Yao[†] and Hua Chun Zeng*[,†,‡]

[†]Department of Chemical and Biomolecular Engineering and KAUST-NUS GCR Program, Faculty of Engineering, National University of Singapore, 10 Kent Ridge Crescent, Singapore 119260

[‡]Institute of Materials Research and Engineering (IMRE), 3 Research Link, Singapore 117602

Supporting Information

ABSTRACT: A synthetic approach has been devised to convert conventional Stöber silica (SiO_2) spheres into a new type of porous structural platform for supporting multicomponent catalysts. With this approach, we have first prepared zinc-doped SiO_2 (Zn-SiO_2) hollow spheres, on which zinc oxide (ZnO) phase and ruthenium (Ru) nanoparticles have been deposited and assembled sequentially in solution phase. A series of complex Ru/ZnO/Zn-SiO_2 nanocatalysts has been thus been integrated onto the zinc-doped SiO_2 supports after additional thermal treatment and reduction. To test their workability under harsh reactive environments, we have further evaluated the above prepared catalysts using arene hydrogenation as model reactions. These integrated nanocatalysts have shown superior activity, high robustness, and easy recovery in the studied heterogeneous catalysis.

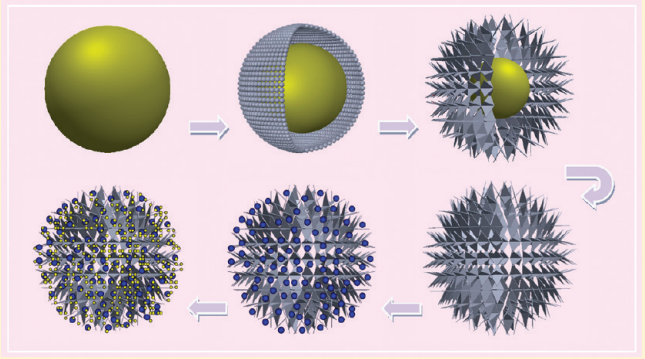

KEYWORDS: *Stöber silica, mesoporous silica, hollow spheres, nanocomposites, Ru nanocatalysts, arene hydrogenation*

INTRODUCTION

Silica (SiO_2) is an important inorganic material, and it has received tremendous research interest over the past decade because of its applications in a vast array of technological fields.[1−7] Among the large research endeavors of this amorphous solid,[1−3] the size-controlled preparation of SiO_2 beads via Stöber protocol in the liquid phase represents a grand example in the field of materials synthesis.[1] Because starting chemicals are low-cost and no organic additives (e.g., surfactants or polymers) are required, solid silica synthesized from Stöber protocol can be prepared rather routinely into monodisperse spheres at a desired size (or diameter), and they have been widely used in self-assembly and fabrication of photonic crystals.[8]

Departing from the above solid silica materials, development of mesoporous bulk silica has also been greatly advanced by utilizing organic supramolecular assemblages.[2,3] With new knowledge of supramolecular chemistry of organic surfactants, research in silica materials entered an entirely new era of development over the past two decades. In recent years, furthermore, such templating methods have been extended to fabrication of core−shell structures with multiple functionalities, where the silica phase is mainly synthesized into shells for molecular screening or metal catalyst protection.[9−13] While many existing porous silica materials (such as MCM-41 and SBA-15) can provide large specific surface areas,[2,3] their surface accessibility could become an issue limiting their applications in certain cases, since any molecules involved in adsorption or reaction have to travel through a long pathway and the actual surface area may not be fully utilized. To circumvent this problem, very recently, high-surface area fibrous SiO_2 spheres with much more open porosity have been prepared.[14] This new type of SiO_2 spheres (named KAUST-1) is very open in nature, yet with a very large specific surface area, have promise as applications as new catalyst supports, where diffusion is thought no longer a limiting step in heterogeneous catalysis.[13] In the meantime, structural transformation of solid SiO_2 spheres prepared by the conventional Stöber protocol into silica hollow spheres or metal-silica yolk-shells has also been achieved by base-etching and dissolution-regrowth process.[15−19] One important feature of these chemically transformed porous SiO_2 materials is that their product monodispersity is very high, since size-control of precursor solid (Stöber silica spheres) can be easily achieved without relying on complex polymer/surfactant templates and/or space confinements of colloidal micelles or vesicles. Apparently, all these recent research advancements have provided diversification of a wide variety of silica-based porous materials to meet different technological needs. Nonetheless, we note that there have been no reports on further utilization of the external surfaces of these newly available SiO_2 hollow spheres for preparation of multicomponent catalysts to work under harsher reaction environ-

Received: August 25, 2011
Revised: November 28, 2011
Published: November 29, 2011

ments (i.e., at high temperature and high pressure),[14−19] in which many well-established heterogeneous catalytic reactions are usually conducted.

As part of our recent research efforts in preparation of porous SiO_2 spheres and hollow functional materials for catalytic applications,[20,21] in this article, we report a hydrothermal approach to chemically modify silica matrix and structurally create interior space and open porosity for conventional Stöber silica spheres. Importantly, this new type of more open lightweight hollow spheres of silica allows us to have a facile integration of active catalytic components onto their external surfaces in a step-by-step manner. We have also tested the workability of the integrated nanocatalysts using arene hydrogenation as model reactions at high reaction temperature and pressure.

EXPERIMENTAL SECTION

Synthesis of SiO_2 Spheres. The SiO_2 spheres used in this work were prepared with a modified Stöber protocol.[1] In a typical process, briefly, 5.0 mL of tetraethylorthosilicate (TEOS, Aldrich, 98%) was dissolved in 92.0 mL of ethanol (Merck, ACS) under stirring, followed by introducing 10.0 mL of ammonia solution (Merck, 25 w%) and then aging for 4 h at room temperature.

Formation of Zn-Doped SiO_2 (Zn-SiO_2) Hollow Spheres. For surface treatment, 1.0 g of the above prepared SiO_2 spheres was dispersed in 200 mL of 2% aqueous diluted poly(diallyldimethylammonium chloride) solution (PDADMAC or PDDA for short, Aldrich, 20 wt %) by ultrasonication and stirred for 30 min. Afterward, 0.05 g of the surface-modified SiO_2 spheres and 0.03 g of $Zn_4CO_3(OH)_6{\cdot}H_2O$ were dispersed in 20.0 mL of deionized water again, followed by hydrothermal treatment at 180 °C for 1−12 h (mostly 5−6 h). After reaction, the autoclave was cooled under tap water, and white silica hollow spheres were separated from the supernatant via centrifugation, followed by drying at 60 °C for 12 h and heating at 350 °C for 2 h.

Preparation of ZnO/Zn-SiO_2 Hollow Spheres. A total of 0.05 g of Zn-SiO_2 hollow spheres and 0.05 g of zinc acetate dihydrate (Scharlau, reagent grade) was dissolved into 40.0 mL of ethanol under stirring, followed by hydrothermal treatment at 180 °C for 1 h.

Synthesis of Ruthenium (Ru) Nanoparticles. Preparation of ruthenium nanoparticles was carried out on the basis of a reported method for the synthesis of PtRu alloy nanoparticles with some modifications.[22] Briefly, 40 mg of ruthenium chloride hydrate (Aldrich, ReagentPlus) and 0.2 g of sodium hydroxide (Merck, GR) was dissolved into 20.0 mL of ethylene glycol (Mallinckrodt, AR) under stirring. Subsequently, the solution was heated to 160 °C and kept for 3 h.

Assembly of Ru/ZnO/Zn-SiO_2, Ru/Zn-SiO_2, and Ru/SiO_2 (Gel) Catalysts. A total of 100 mg of ZnO/Zn-SiO_2 or 100 mg of Zn-SiO_2 hollow spheres or 1.00 g of commercial SiO_2 (gel) powder (Aldrich, technical grade, pore size 60 Å, 200−425 mesh) was dispersed in 2.0−20.0 mL of ethanol by ultrasonication, followed by introducing 0.1−5.0 mL of as-prepared Ru colloidal solution under vigorous stirring. After 3 h of stirring, the resultant Ru/ZnO/Zn-SiO_2, Ru/Zn-SiO_2, or Ru/SiO_2 (gel) catalysts were washed with ethanol twice.

Hydrogenation Reaction of Arenes. Prior to the hydrogenation reaction, the catalysts were activated at 300 °C for 2 h in H_2 atmosphere in a tubular electric furnace. Afterward, a defined amount of (mostly 100 mg; see Table 1 in the main text for a special case of 520 mg) catalysts, 50.0 mL of aromatic substrates, such as toluene (Merck, AR), benzene (Sigma-Aldrich, anhydrous, 99.8%), or *m*-xylene (Sigma-Aldrich, Reagent-plus), and 1.0 mL of decane (Alfa Aesar, 99%) were introduced into a Parr 4843 reactor. The reactor was then purged with high purity H_2 (>99.99%, Singapore Oxygen Air Liquide Pte Ltd.) for 15 min, and hydrogenation reaction was carried out at 130 °C with H_2 pressure of 4 MPa.

Materials Characterization. The crystallographic structures of the above catalytic materials were determined by X-ray diffraction (XRD; Shimadzu XRD-6000, Cu Kα). The spatial, morphological, and compositional studies were carried out with scanning electron microscopy and energy-dispersive X-ray spectroscopy (SEM/EDX, JSM-5600LV), transmission electron microscopy (TEM; JEM-2010 and JEM-2100F), X-ray fluorescence spectroscopy (XFS), and X-ray photoelectron spectroscopy (XPS; AXIS-HSi, Kratos Analytical). Electrokinetic potentials of the silica sphere suspensions were measured with ZetaPlus4 Brookhaven zeta potential analyzer. Measurements of specific surface area and porosity analysis for silica spheres were performed using N_2 adsorption−desorption isotherms (Quantachrome NOVA-3000). Reactants and products in toluene hydrogenation were analyzed using gas chromatograph (Agilent 7890A series GC) and GC-mass spectrometry (HP 6890 GC system and HP 5973 mass selective detector).

Table 1. Arene Hydrogenations (Mostly Toluene Hydrogenation unless Otherwise Specified; Ru Content in wt %)

entry	Ru catalysts	T (min)	conversion (%)[i]	TOF (h^{-1})[j]
1	3.2 Ru% catalyst[a]	70	100	1.3×10^4
2	1.4 Ru% catalyst[a]	120	100	1.7×10^4
3	1.2 Ru% catalyst[b]	120	100	2.0×10^4
4	3.2 Ru% catalyst[c]	120	60.1	4.5×10^3
5	10.0 Ru% catalyst[c]	120	56.2	1.3×10^3
6	2.6 Ru% catalyst[a,d]	60	100	1.1×10^4
7	1.6 Ru% catalyst[a,e]	60	53.7	9.6×10^3
8	1.1 Ru% catalyst[a,f]	60	88.0	4.4×10^3
9	2.6 Ru% catalyst[a,g]	30	100	2.6×10^4
10	2.6 Ru% catalyst[a,h]	60	86.3	8.2×10^3

[a]Ru/ZnO/Zn-SiO_2 activated in H_2 at 300 °C for 2 h before hydrogenation reaction. [b]Ru/ZnO/Zn-SiO_2 activated in H_2 at 300 °C for 5 h before hydrogenation reaction. [c]Ru/ZnO/Zn-SiO_2 without H_2 pretreatment. [d]Ru/ZnO/Zn-SiO_2 in the 5th run of hydrogenation reaction. [e]Catalyst without ZnO deposition (i.e., Ru/Zn-SiO_2). [f]Commercial SiO_2-gel-supported Ru catalyst without ZnO deposition (i.e., Ru/SiO_2 (gel); 520 mg catalyst was used in this reaction due to its low activity). [g]Ru/ZnO/Zn-SiO_2 for benzene hydrogenation. [h]Ru/ZnO/Zn-SiO_2 for *m*-xylene hydrogenation. [i]Conversion of substrates to corresponding hydrogenated products. [j]Turnover frequency (TOF) is defined as the number of mol of converted substrates per mol of Ru per hour.

RESULTS AND DISCUSSION

Figure 1 shows surface modification and some major synthetic steps for preparation of this new type of porous SiO_2 supports, starting from Stöber SiO_2 spheres. In Figure 2a,b, monodisperse SiO_2 spheres were prepared with Stöber protocol.[1] These precursor solid spheres were first decorated with a layer of cationic polyelectrolyte, poly(diallyldimethylammonium chloride) (PDDA, Figure 1a). It should be mentioned that the actual function of positively charged PDDA used for hollowing silica spheres is quite different from other reported synthetic strategies in which nonionic neutral polymeric ligands (e.g., poly(vinylpyrrolidone) (PVP)) served as a surface protecting agent while a strong base (e.g., NaOH) functioned as an etchant to obtain porosity.[17] The purpose of using PDDA herein was to alter the surface charge of native silica spheres and to further improve dispersity of the silica spheres in deionized water.[14] It has been well-known that the surfaces of silica spheres obtained via Stöber method are covered with hydroxyl ions and thus exhibit negative charges. After the adsorption of PDDA, we were able to change surface charges of the silica from negative to positive. Our zeta-potential measurement reveals that the electro-kinetic potential increased from initial −48.0 mV to +38.5 mV when the PDDA was

dx.doi.org/10.1021/cm2030119 | Chem. Mater. 2012, 24, 140−148

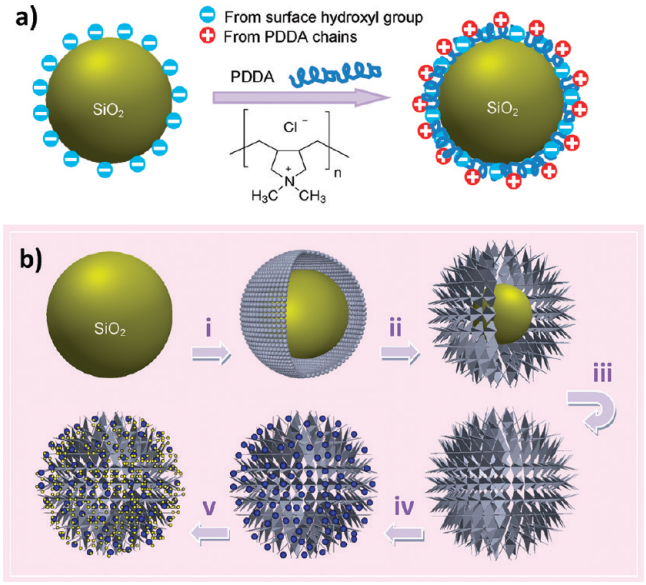

Figure 1. (a) Modification of SiO_2 surface with PDDA: electrostatic attraction between negative hydroxyl groups and positive charges of PDDA and (b) illustration of this synthetic approach to fabricate integrated nanocatalysts: (i) modify surface of SiO_2 (see (a)) and create yolk (pure SiO_2, dark green)−shell (Zn-doped SiO_2, gray), (ii) reduce yolk size, (iii) form plate-interlaced Zn-doped SiO_2 hollow sphere, (iv) deposit ZnO nanoparticles (blue dots), and (v) add Ru nanoparticles (small yellow dots). Note that (i) to (iii) belong to "top-down" steps while (iv) and (v) are "bottom-up" steps.

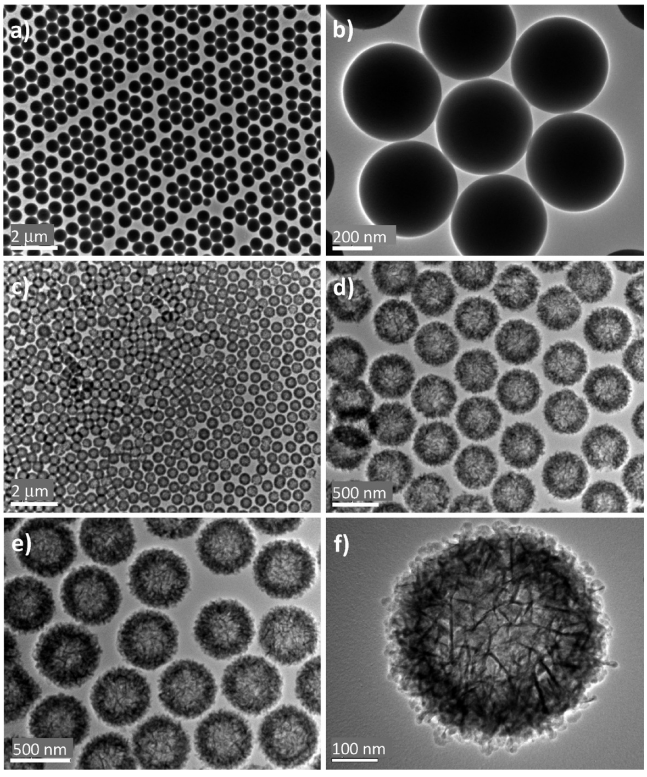

Figure 2. Transmission-electron-microscopy (TEM) images of (a, b) solid SiO_2 spheres synthesized by Stöber protocol and (c−f) porous Zn-doped SiO_2 (Zn-SiO_2) hollow spheres prepared by the present approach.

adsorbed on the pristine SiO_2 spheres via electrostatic attraction. Furthermore, the PDDA-coated SiO_2 spheres can be dispersed better in aqueous solution, and they do not aggregate even at high temperatures compared to their uncoated counterparts. As another piece of information and unlike those protected by nonionic PVP,[16,17] the PDDA-adsorbed silica spheres were entirely broken down when using NaOH as an etchant under our synthetic conditions (Supporting Information, SI-1). It is thus affirmed that PDDA does not simply function as a protecting agent in the basic environment. The PDDA-adsorbed SiO_2 spheres were then hydrothermally treated with zinc carbonate hydroxide ($Zn_4CO_3(OH)_6{\cdot}H_2O$),[23] after which Zn-doped SiO_2 (Zn-SiO_2) hollow spheres could be harvested easily from their supernatant. Displayed in Figure 2c−f, the Zn-SiO_2 spheres still maintained a spherical morphology and did not change much in size. At high image magnifications, it is found that the hollow spheres consist of interlaced flakes that form different sized pores, and the surfaces are very open (Figure 2f). Consistent with this observation, the specific surface area of the Zn-SiO_2 hollow spheres was determined to be 268 m^2/g (with the BET method). Our texture and porosity characterization in Figure 3 shows that the nitrogen adsorption−desorption isotherms belongs to typical *H*3 hysteresis loop, which is normally attributed to presence of disordered mesopores (e.g., nonrigid aggregates of plate-like particles or assemblages of slit-shaped pores).[24] However, there is also a certain adsorbed volume at very low relative pressure (P/P_0) range, which can be assigned to the N_2 in micropores and/or on the surfaces of silica spheres. A delayed desorption at ca. P/P_0 = 0.45−0.48 (indicated with a blue arrow in Figure 3a) in this hysteresis loop should be associated with the critical instability of the meniscus or tensile strength effect (TSE).[24] The steep rise of the adsorption branch near P/P_0 = 0.9 indicates the presence of relatively large mesopores with the diameter of 10 nm. In good agreement with the direct TEM observation in Figure 2f, the pore size distribution shown in Figure 3b was determined from the desorption curve with Barett−Joyner−Halenda (BJH; based on the macroscopic Kelvin equation) method. As expected, a wide variety of mesopores ranging from ca. 3 to 50 nm was revealed. Nonetheless, the sharp peak located at 3.8 nm should be considered as an artifact due to the delayed desorption discussed above.[24] In order to obtain more insight on the real picture of the modified pore structure, the BJH pore size distribution was also estimated from the data of the adsorption branch of this sample (Figure 3a). In Figure 3c, the pore size profile indeed reveals a significant presence of small mesopores over the diameter range of 3−10 nm. Further investigation was carried out to understand the mechanism of this hollowing process. In Figure 4a−b, with a short reaction time of 2−3 h, it is obvious that the exterior of the silica spheres was first reconstructed to form a core−shell and then to a yolk−shell structure. The shells are loose and consist of many tiny thin flakes. A longer reaction time led to reduction in yolk size and generation of more interior space between the yolk and shell (Figure 4c−d). Meanwhile, the pristine silica gradually dissolved and regrew into interlaced flakes that structured the shells. Finally, porous Zn-SiO_2 spheres with a large central void were fabricated (e.g., Figure 2c−f). Besides those shown in Figure 2, the resultant SiO_2 core−shell, yolk−shell, or hollow spheres are highly monodisperse, and they can be easily arranged into superlattice assemblages, as exemplified in Figure 5. Quite interestingly, uniform intersphere spaces could also be generated from these orderly arranged superlattices in order to attain even more complex hierarchical pore structures, though this is not the main objective of the present work.

dx.doi.org/10.1021/cm2030119 | *Chem. Mater.* 2012, 24, 140−148

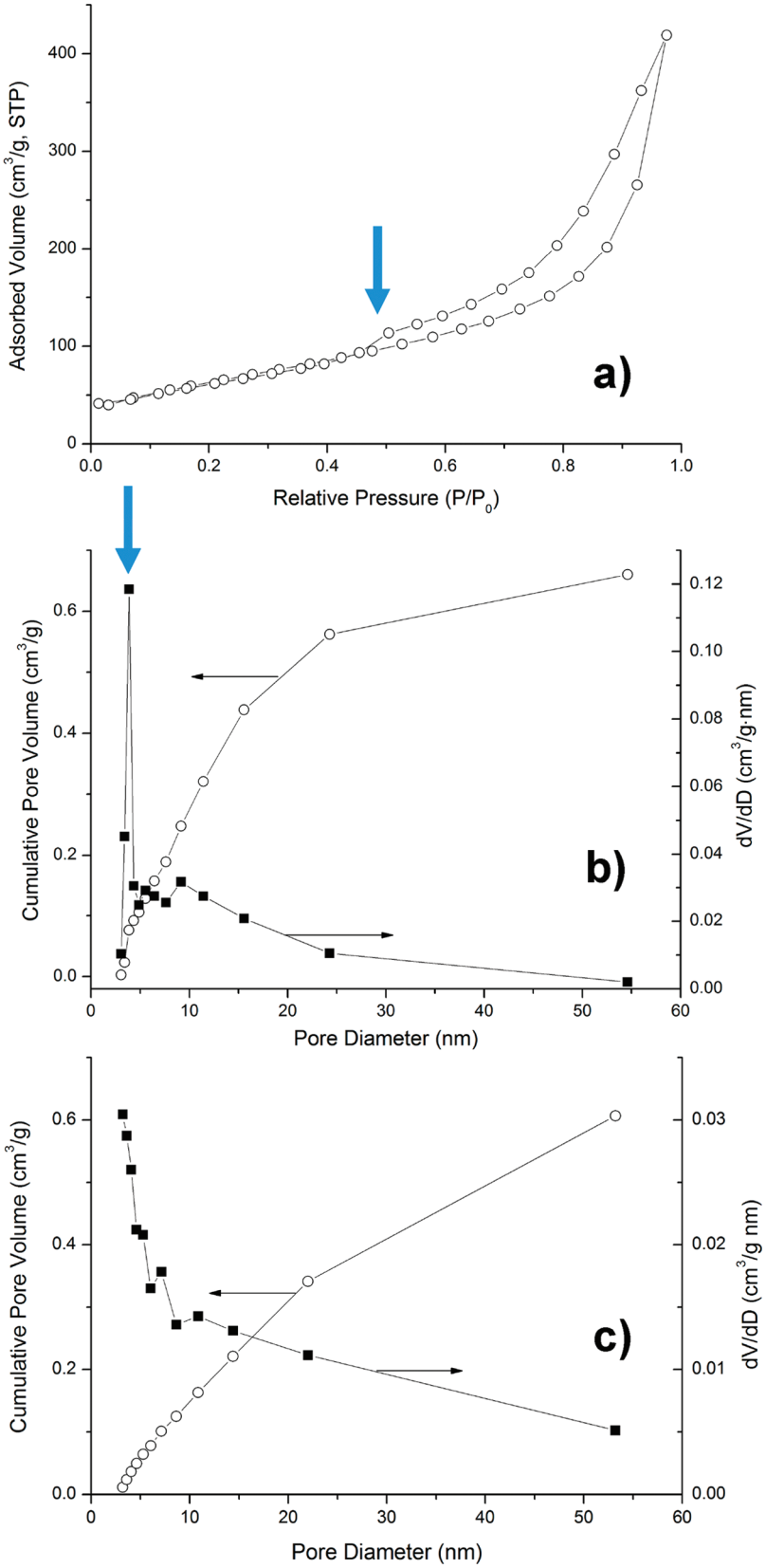

Figure 3. BET/BJH analytical results of porous Zn-doped SiO_2 (Zn-SiO_2) spheres: (a) nitrogen adsorption−desorption isotherms (for BET analysis), (b) pore volume curve and pore size distribution profile calculated from desorption isotherm (with BJH method; note: due to the critical instability of the meniscus or tensile strength effect (TSE; the onset of cavitation was indicated by a blue arrow in (a)), the sharp peak at 3.8 nm (marked with a blue arrow in (b)) could be considered as an artifact,[24] and (c) pore volume curve and pore size distribution profile calculated from adsorption isotherm (with BJH method).

As a key chemical to this work, $Zn_4CO_3(OH)_6{\cdot}H_2O$ provided a basic environment by releasing hydroxyl anions during the hydrothermal treatment. Under this condition, on the one hand, the positive PDDA-adsorbed silica actually

dx.doi.org/10.1021/cm2030119 | *Chem. Mater.* 2012, 24, 140−148

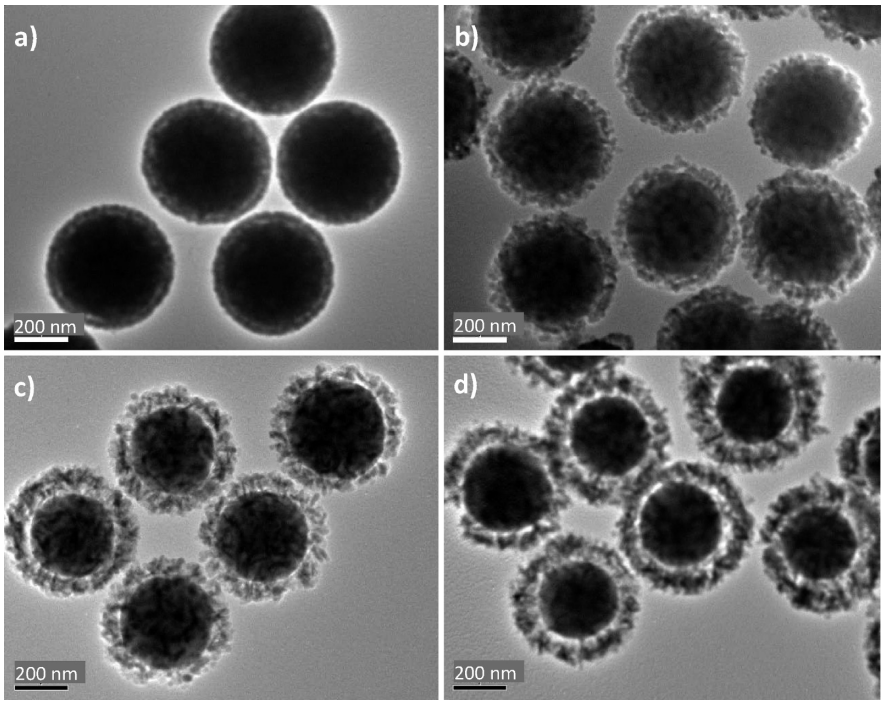

Figure 4. TEM images of as-prepared Zn-SiO_2 spheres after different reaction times: (a) 2 h, (b) 3 h, (c) 4 h, and (d) 5 h using the present method.

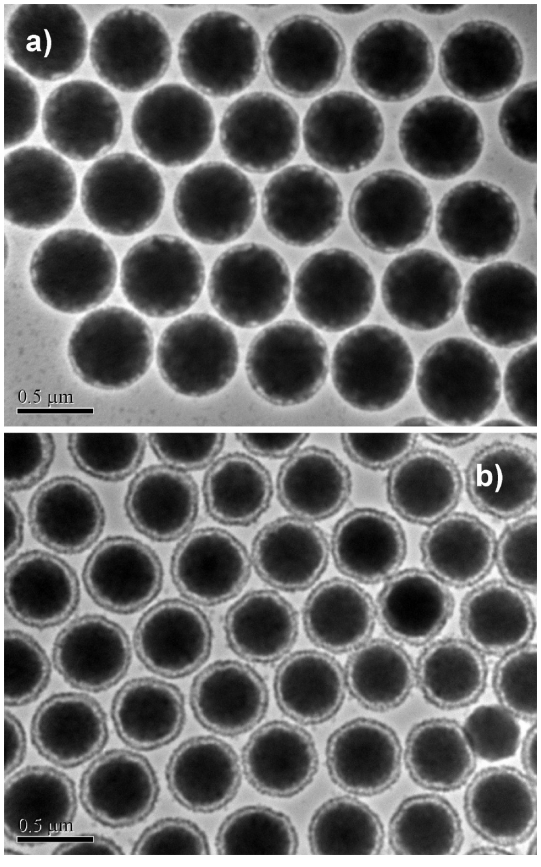

Figure 5. Highly monodisperse Zn-SiO_2 core–shell (a) and yolk–shell (b) structures which form two-dimensional hexagonal arrays.

became more inviting to the negative hydroxyl anions owing to their opposite electrostatic attraction, as evidenced in our zeta-potential analysis. In this regard, PDDA adsorption is an indispensable step to the hollowing process. On the other hand, the intricate nature of this polymer would also exert a physical diffusion barrier for the hydroxyl anions to penetrate through and ensure a steady influx of the anions around an entire SiO_2 sphere, also serving as an organic template for the reconstruction of the SiO_2 spheres. The role of this polyelectrolyte was further investigated: when the PDDA used in the synthesis was insufficient, the shape of Zn-SiO_2 shell could not be taken (Supporting Information, SI-2), because of limited PDDA on the surfaces to attract hydroxyl ions and to serve as a templating material at the same time. However, the PDDA-adsorbed silica spheres would remain unchanged when the PDDA was too much during the hydrothermal treatment since any additional PDDA in the bulk solution also directly attracted the hydroxyl anions in the same solution phase (Supporting Information, SI-2). In this approach, it has been demonstrated that the pristine silica phase went through a number of stages (Figures 1 and 4). Apart from surface change, in particular, dissoluting silica in the form of silicate oligomers (soluble anions)[25] could deposit back to porous shells when they diffused from the inside out (i.e., matter relocation from yolk to shell). In this way, the size of the inner silica yolk can be virtually tuned from zero to several hundred nanometers by simply adjusting the reaction time. Taking advantage of the Stöber protocol (which allows a fine-tuning over the size of solid SiO_2 precursors), our hollowing strategy also shows a generality to handle the silica spheres at different sizes and thus to achieve the size control for the resultant hollow spheres of SiO_2. In Figure 6, in addition to those reported in Figure 2, we have also successfully transformed smaller solid SiO_2 beads into open porous hollow or yolk–shell spheres (not shown, since they are solid intermediates of the hollow structures) in the diameter range of only 150–250 nm, noting that shell structures can also be fine-tuned by varying the above-mentioned synthetic parameters.

Besides the structural transformation, $Zn_4CO_3(OH)_6{\cdot}H_2O$ also introduced transition metal dopant (Zn^{2+}) to hollow

dx.doi.org/10.1021/cm2030119 | *Chem. Mater.* 2012, 24, 140–148

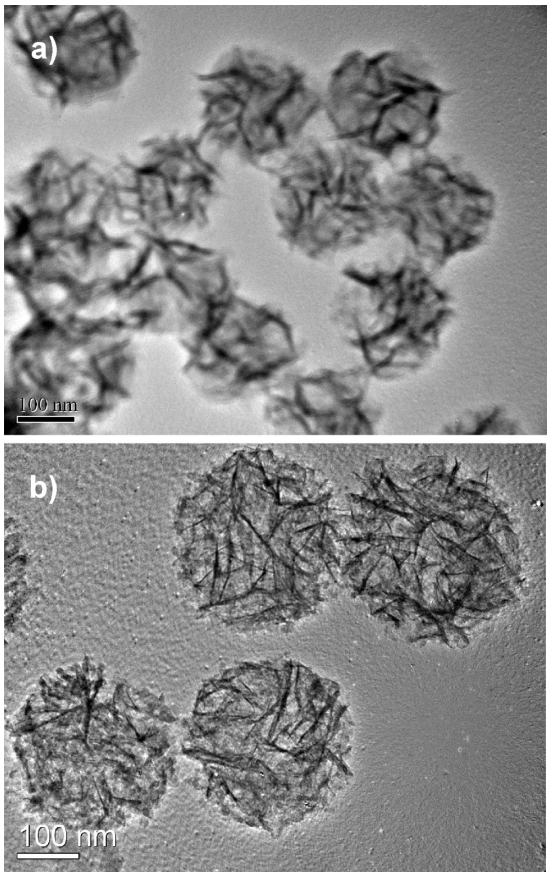

Figure 6. Generality of this preparative approach which can form small-sized Zn-SiO_2 hollow spheres: (a) 150 nm in average diameter and (b) 250 nm in average diameter.

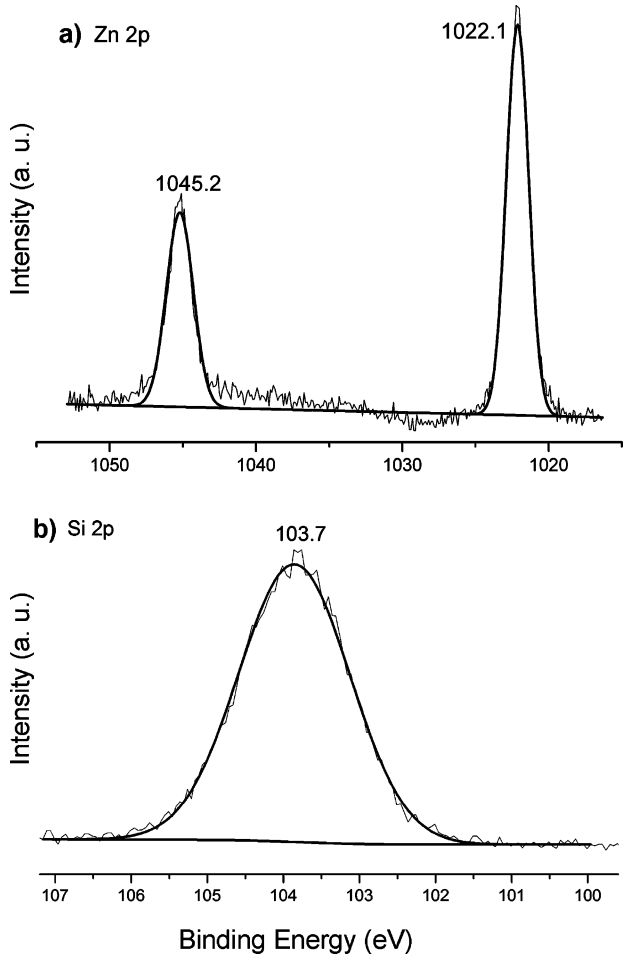

Figure 7. XPS surface analysis of porous Zn-doped SiO_2 (Zn-SiO_2) spheres: (a) Zn 2p and (b) Si 2p photoelectrons.

spheres of silica. Our X-ray fluorescence spectroscopy (XFS, Supporting Information, SI-3) study indicates that 8.5% of the starting zinc had been incorporated into the SiO_2 phase in this hollowing process (atomic ratio of Zn:Si ≈ 3:100 in the final Zn-SiO_2, Supporting Information, SI-3). Again, our X-ray photoelectron spectroscopy (XPS) investigation in Figure 7a affirms that there are divalent zinc cations in the SiO_2 shells. Moreover, we have observed that binding energies of Zn $2p_{1/2}$ and Zn $2p_{3/2}$ photoelectrons are shifted noticeably to the positive side at 1045.2 and 1022.1 eV, respectively, compared to those of phase-pure ZnO at 1044.2 and 1021.2 eV,[23,26] indicating that Zn^{2+} cations have been incorporated into silica matrix, and given rise to Zn−O−Si linkages (Si 2p, Figure 7b). The XPS analysis reveals that there is an enrichment of zinc element in the surface region (atomic ratio of Zn:Si ≈ 1:5), which is understandable in view of a large difference between Zn and Si in their oxidation states (+2 vs +4). The presence of surface Zn^{2+} would likely benefit the introduction of a secondary phase that has a similar chemical constituent or structure. For example, a ZnO layer can be more facilely integrated into the Zn-SiO_2 substrate where the Zn^{2+} cations in the Zn−O−Si linkages would naturally serve as initial nucleation sites for the growth of ZnO (zinc acetate was used as a precursor for ZnO deposition; Experimental Section). Our TEM investigation shows that a layer of size-controlled ZnO crystallites can be uniformly deposited on the silica shells. The development of wurtzite-type ZnO is also confirmed in the X-ray diffraction (XRD) pattern of Figure 8a (JCPDS card no. 36-1451; space group $P6_3mc$; lattice constants a_o = 3.25 Å and c_o = 5.21 Å);[23,26] note that the Zn-SiO_2 hollow spheres are amorphous and are shown in the background of the ZnO diffraction pattern. The average size of crystallites in the deposit layer of ZnO is 8.3 nm, determined by the Scherrer equation with the (101) diffraction peak. As an additional note, freestanding ZnO crystallites were not present in the solution, suggesting that this metal oxide was site-specifically deposited on the Zn-SiO_2 spheres. Similar to those shown in Figure 3a, we have also measured the nitrogen adsorption−desorption isotherms for the ZnO/Zn-SiO_2 sample (Supporting Information, SI-4). The BET specific surface area of this sample is still as high as 187.5 m^2/g, despite the deposition of the ZnO overlayer. Nevertheless, the lowering in surface area can be attributed to partial blocking of small mesopores by the ZnO crystallites. Similar to that shown in Figure 3c, the BJH pore size distribution was also determined from the adsorption branch (Supporting Information, SI-4). As expected, most of pores concentrate in the range between 5 and 45 nm, and the intensity of diameter smaller than 5 nm decreases significantly (Supporting Information, SI-4), which is quite different from the pore size distribution of the Zn-doped silica hollow spheres of Figure 3c. Considering this difference, it is thus convincing that the pristine pore structure of Zn-SiO_2 spheres has been modified and their smaller mesopores are indeed partially blocked by surface layer of ZnO.

With the above ZnO/Zn-SiO_2 composite as a structural platform, in principle, a third or even a fourth component could

dx.doi.org/10.1021/cm2030119 | *Chem. Mater.* 2012, 24, 140−148

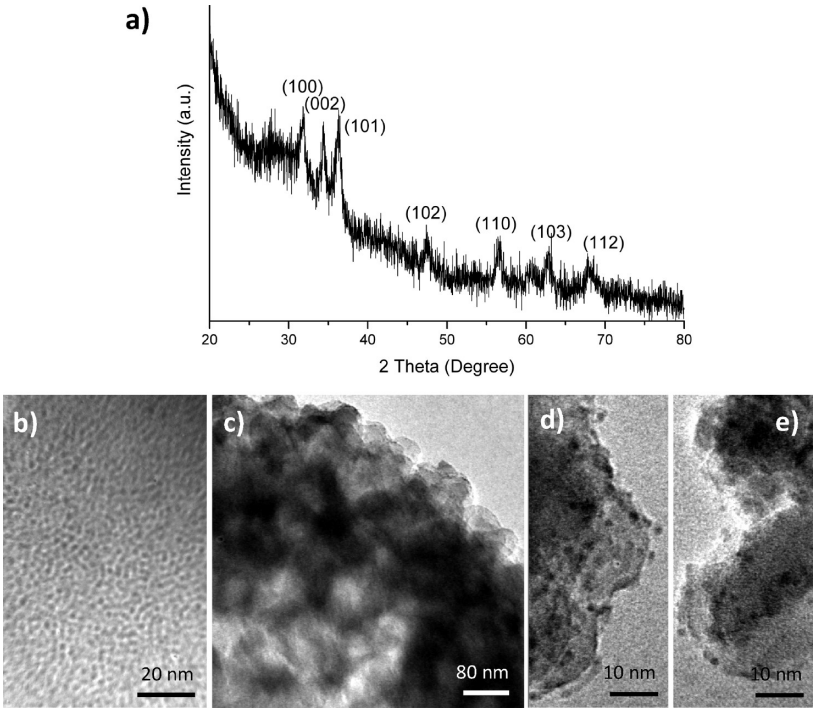

Figure 8. (a) XRD pattern of Ru/ZnO/Zn-SiO_2 catalyst spheres, (b) TEM image of as-synthesized Ru nanoparticles, (c) TEM image of an as-prepared Ru/ZnO/Zn-SiO_2 catalyst sphere (only 1/4 is shown), and (d and e) detailed views of Ru nanoparticles anchored on the outmost surfaces of Ru/ZnO/Zn-SiO_2.

be introduced sequentially if one wishes to pursue integration of multicomponent nanocatalysts. In this regard, as a trial example in the present work, ruthenium (Ru) was selected as a third component to add onto the binary composite considering its wide applications in heterogeneous catalysis.[22] Instead of prevailing impregnation-then-calcination methods for loading catalytic metals, herein we developed a self-assembly approach to integrate Ru onto the composite support ZnO/Zn-SiO_2 (Experimental Section), which allows a better control of the particle size, morphology, and depositing location.[27] Shown in Figure 8b, our as-prepared Ru nanoparticles are highly uniform with an average particle size at 2.2 ± 0.3 nm. Unlike other common methods used to prepare metal nanoparticles, our approach does not require additional surfactants to constrain the particle growth. Therefore, these Ru nanoparticles were highly dispersible in polar solvents, and they could be simply added into an alcoholic suspension of ZnO/Zn-SiO_2 under vigorous stirring. Figure 8c–e show that the Ru nanoparticles were evenly distributed around the ZnO/Zn-SiO_2 shells. A desired amount of deposited ruthenium could be controlled by added volume of Ru suspension and determined with energy-dispersive X-ray spectroscopy (EDX) method rather conveniently.

After the above integration of the metal catalyst onto the ZnO/Zn-SiO_2, a number of ternary Ru/ZnO/Zn-SiO_2 composite catalysts were obtained. In order to test the applicability of the integrated catalysts under harsh reaction environments, we evaluated their catalytic activity on hydrogenation of toluene (which is normally conducted under high temperature and high pressure) in comparison with the literature data. Because of easy oxidation of Ru nanoparticles in air, the catalysts were pretreated in a hydrogen stream at 300 °C to remove surface oxide and enhance binding between the Ru and ZnO prior to the reaction. Performance of the catalysts with different Ru loadings and treatments is reported in Figure 9a and Table 1. Compared to supported or unsupported Ru nanoparticles,[28,29] quite encouragingly, our catalysts exhibit superior activities in this model reaction. In Table 1, for example, our catalysts display very high turnover frequencies (TOF) in the range of 1.3×10^3 to 2.0×10^4 h^{-1}. The observed hydrogenation selectivity of toluene to methyl-cyclohexane is 100% (Supporting Information, SI-5).[30] The reason for their remarkable catalytic performance can be attributed to small uniform metal particles, high specific surface area, short-diffusion paths, and synergistic effects arising from the active metal (Ru) and its support (ZnO/Zn-SiO_2). The Ru/ZnO/Zn-SiO_2 system is also robust in catalytic cycles (Table 1). Shown in Figure 9b and the Supporting Information (SI-6), Ru nanoparticles in our used catalysts still remain highly dispersed while their average particle size only increases slightly (2.5 ± 0.2 nm). Apparently, controllability over catalyst loading and dispersity is significantly improved using this integrative approach. Quite different from those prepared with conventional impregnation methods or confined within porous materials,[31] our Ru nanoparticles are quite monodisperse and can be loaded directly onto the large surfaces of catalyst support. Furthermore, this expensive metal commodity can be better utilized, as agglomeration of metal can be effectively avoided; yet mass transport is unlikely to be a limiting step in the catalysts, as their pores are more open, compared with normal mesoporous silica supports. Despite its supporting role, the sandwiched ZnO layer in the final Ru/ZnO/Zn-SiO_2 likely also contributes to the overall catalytic activity of hydrogenation. For instance, together with active Ru phase, Lewis acid sites of unsaturated defects such as vacancies, atomic steps, kinks, and terraces on the ZnO crystallite surfaces may favor adsorption of toluene and stabilize reaction intermediates (such as spillover hydrogen from Ru), noting that the (0001)

dx.doi.org/10.1021/cm2030119 | *Chem. Mater.* 2012, 24, 140–148

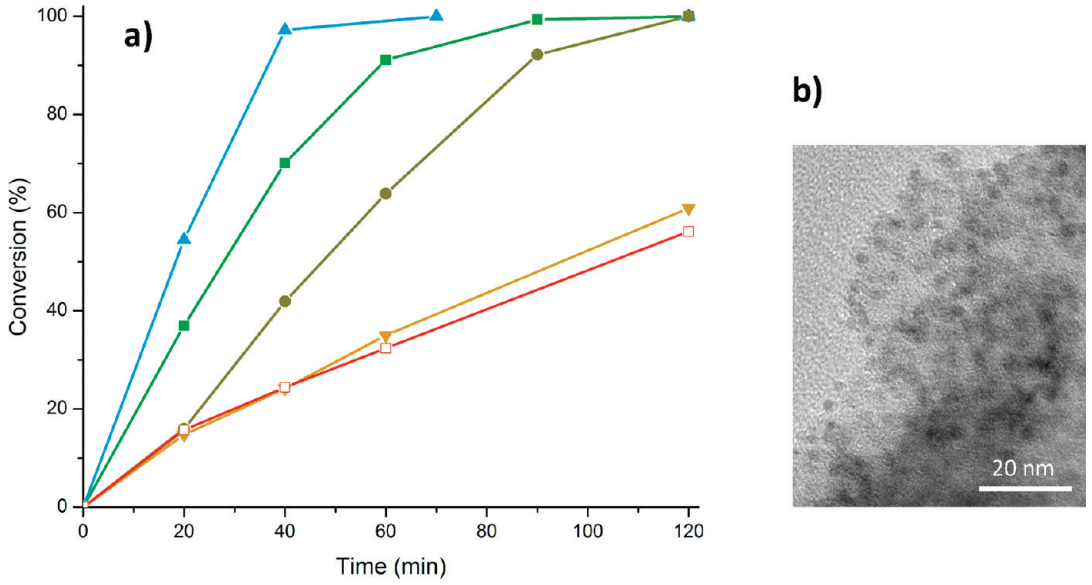

Figure 9. (a) Toluene hydrogenation: ▲ 3.2 Ru% catalyst was activated in H_2 at 300 °C for 2 h, followed by hydrogenation at 130 °C under 4 MPa, ■ 1.4 Ru% catalyst was activated in H_2 at 300 °C for 2 h, followed by hydrogenation at 130 °C under 4 MPa, ● 1.2 Ru% catalyst was activated in H_2 at 300 °C for 5 h, followed by hydrogenation at 130 °C under 4 MPa, ▼ 3.2 Ru% nonactivated catalyst at 130 °C under 4 MPa, □ 10.0 Ru% nonactivated catalyst at 110 °C under 4 MPa; and (b) TEM image of a used catalyst (▲) after the reaction in (a).

facets of ZnO are positively charged (i.e., Lewis acid sites). It has been known that Lewis acids can activate aromatic rings.[32,33] In the absence of the ZnO phase, indeed, the TOF of arene hydrogenation is unambiguously lower. As shown in Table 1, the catalyst Ru/Zn-SiO_2 (without a ZnO interlayer, Entry 7) has a poorer catalytic activity than Ru/ZnO/Zn-SiO_2 (Entries 1, 2, and 3). Furthermore, we have attempted to change the substrate from hollow spheres to commercial silica gel (Entry 8). The TOF value of this catalyst (Entry 8) is only half that of the Ru/Zn-SiO_2 hollow spheres (Entry 7). Therefore, the ZnO deposition and silica hollow structures are indeed essential for good catalytic activity in this reaction. The synergistic effects and actual functions of the solid phases in this complex catalyst system are currently under further investigation.

Finally, it should be mentioned that, apart from the particle size uniformity, another two structural merits of the above catalysts with a hollow interior are that they are lightweight and have an open accessibility. Understandably, these unique features are able to lighten sediment problems caused by gravity yet allow reactants and products together with solvents to be more freely moving in and out of the central interior. On the one hand, in this regard, the lightweight hollow-sphere catalysts can be conceptually considered as curled two-dimensional "sheet-like" materials floating in the reaction medium upon mechanical stirring and/or fluidic convections, reducing concentration gradients of chemical species involved in reactions. On the other hand, these organized spherical catalysts have sufficiently large overall particle sizes for an easy separation after use, despite the presence of complex nanoarchitectures (i.e., active catalytic components) in their shells.

CONCLUSIONS

In summary, we have developed an effective hydrothermal process to chemically modify and structurally transform conventional Stöber silica spheres into transition metal doped SiO_2 hollow spheres with more open mesoporosities. Using the porous Zn-doped SiO_2 hollow spheres as a new type of catalyst supports, in particular, we have also fabricated complex Ru/ZnO/Zn-SiO_2 nanocomposites in a stepwise manner; the integrated multicomponent nanocatalysts have shown superior activity in general arene hydrogenation. We have further demonstrated high controllability, sufficient robustness, and easy recovery of these catalysts in the harsh environments of heterogeneous catalysis. In principle, as reported in this work, this new type of SiO_2 hollow spheres can serve as a supporting platform for fabrication of multicomponent nanocatalysts through designed integration.

ASSOCIATED CONTENT

Supporting Information

Additional experimental conditions, XFS and TEM analyses, and catalyst evaluation data of arene hydrogenation. This material is available free of charge via the Internet at http://pubs.acs.org.

AUTHOR INFORMATION

Corresponding Author

*E-mail: chezhc@nus.edu.sg.

ACKNOWLEDGMENTS

The authors acknowledge financial support from National University of Singapore, Singapore, and King Abdullah University of Science and Technology, Saudi Arabia.

REFERENCES

(1) Stöber, W.; Fink, A.; Bohn, E. *J. Colloid Interface Sci.* **1968**, *26*, 62.
(2) Kresge, C. T.; Leonowicz, M. E.; Roth, W. J.; Vartuli, J. C.; Beck, J. S. *Nature* **1992**, *359*, 710.
(3) Zhao, D. Y.; Feng, J. L.; Huo, Q. S.; Melosh, N.; Fredrickson, G. H.; Chmelka, B. F.; Stucky, G. D. *Science* **1998**, *279*, 548.
(4) Fan, J.; Yu, C. Z.; Gao, T.; Lei, J.; Tian, B. Z.; Wang, L. M.; Luo, Q.; Tu, B.; Zhou, W. Z.; Zhao, D. Y. *Angew. Chem., Int. Ed.* **2003**, *42*, 3146.
(5) Che, S.; Liu, Z.; Ohsuna, T.; Sakamoto, K.; Terasaki, O.; Tatsumi, T. *Nature* **2004**, *429*, 281.

(6) Zhu, Y. F.; Shi, J. L.; Shen, W. H.; Dong, X. P.; Feng, J. W.; Ruan, M. L.; Li, Y. S. *Angew. Chem., Int. Ed.* **2005**, *44*, 5083.
(7) Wan, Y.; Wang, H. Y.; Zhao, Q. F.; Klingstedt, M.; Terasaki, O.; Zhao, D. Y. *J. Am. Chem. Soc.* **2009**, *131*, 4541.
(8) Wang, W.; Gu, B. H.; Liang, L. Y.; Hamilton, W. A. *J. Phys. Chem. B* **2003**, *107*, 12113.
(9) Deng, Y. H.; Qi, D. W.; Deng, C. H.; Zhang, X. M.; Zhao, D. Y. *J. Am. Chem. Soc.* **2008**, *130*, 28.
(10) Joo, S. H.; Park, J. Y.; Tsung, C. K.; Yamada, Y.; Yang, P. D.; Somorjai, G. A. *Nat. Mater.* **2009**, *8*, 126.
(11) Cauda, V.; Schlossbauer, A.; Kecht, J.; Zürner, A.; Bein, T. *J. Am. Chem. Soc.* **2009**, *131*, 11361.
(12) Zhang, F.; Braun, G. B.; Shi, Y. F.; Zhang, Y. C.; Sun, X. H.; Reich, N. O.; Zhao, D. Y.; Stucky, G. D. *J. Am. Chem. Soc.* **2010**, *132*, 2850.
(13) Deng, Y. H.; Cai, Y.; Sun, Z. K.; Liu, J.; Liu, C.; Wei, J.; Li, W.; Liu, C.; Wang, Y.; Zhao, D. Y. *J. Am. Chem. Soc.* **2010**, *132*, 8466.
(14) Polshettiwar, V.; Cha, D.; Zhang, X. X; Basset, J. M. *Angew. Chem., Int. Ed.* **2010**, *49*, 9652.
(15) Kamata, K.; Lu, Y.; Xia, Y. N. *J. Am. Chem. Soc.* **2003**, *125*, 2384.
(16) Ge, J.; Zhang, Q.; Zhang, T.; Yin, Y. *Angew. Chem., Int. Ed.* **2008**, *47*, 8924.
(17) Zhang, Q.; Zhang, T.; Ge, J.; Yin, Y. *Nano Lett.* **2008**, *8*, 2867.
(18) Zhang, T. R.; Ge, J. P.; Hu, Y. X.; Zhang, Q.; Aloni, S.; Yin, Y. D. *Angew. Chem., Int. Ed.* **2008**, *47*, 5806.
(19) Wong, Y. J.; Zhu, L. F.; Teo, W. S.; Tan, Y. W.; Yang, Y. H.; Wang, C.; Chen, H. Y. *J. Am. Chem. Soc.* **2011**, *133*, 11422.
(20) Wang, D. P.; Zeng, H. C. *Chem. Mater.* **2009**, *21*, 4811.
(21) Wang, D. P.; Zeng, H. C. *Chem. Mater.* **2011**, *23*, 4886.
(22) Bock, C.; Paquet, C.; Couillard, M.; Botton, G. A.; MacDougall, B. R. *J. Am. Chem. Soc.* **2004**, *126*, 8028.
(23) Yao, K. X.; Zeng, H. C. *Langmuir* **2008**, *24*, 14234.
(24) Thommes, M. Physical Adsorption Characterization of Ordered and Amorphous Mesoporous Materials. In *Nanoporous Materials: Science and Engineering*; Lu, G. Q., Zhao, X. S., Eds.; Imperial College Press: Oxford, 2004; Chapter 11, p 317.
(25) Rimer, J. D.; Trofymluk, O.; Navrotsky, A.; Lobo, R. F.; Vlachos, D. G. *Chem. Mater.* **2007**, *19*, 4189.
(26) Yao, K. X.; Sinclair, R.; Zeng, H. C. *J. Phys. Chem. C* **2007**, *111*, 2032.
(27) Li, J.; Zeng, H. C. *Chem. Mater.* **2006**, *18*, 4270.
(28) Milone, C.; Neri, G.; Donato, A.; Musolino, M. G.; Mercadante, L. *J. Catal.* **1996**, *159*, 253.
(29) Nowicki, A.; Le Boulaire, V.; Roucoux, A. *Adv. Synth. Catal.* **2007**, *349*, 2326.
(30) Zahmakıran, M.; Tonbul, Y.; Özkar, S. *J. Am. Chem. Soc.* **2010**, *132*, 6541.
(31) Deng, W.; Liu, M.; Tan, X.; Zhang, Q.; Wang, Y. *J. Catal.* **2010**, *271*, 22.
(32) Koltunov, K. Y.; Prakash, G. K. S.; Rasul, G.; Ohah, G. A. *Tetrahedron* **2002**, *58*, 5423.
(33) Liu, H. Z.; Jiang, T.; Han, B. X.; Liang, S. G.; Zhou, Y. X. *Science* **2009**, *326*, 1250.